

A search for solar-like oscillations and granulation in α Cen A

H. Kjeldsen,^{1,2} T. R. Bedding,³ S. Frandsen² and T. H. Dall²

¹Teoretisk Astrofysik Center, Danmarks Grundforskningsfond (hans@obs.aau.dk)

²Institute of Physics and Astronomy, Aarhus University, DK-8000 Aarhus C, Denmark

³Chatterton Astronomy Department, School of Physics, University of Sydney 2006, Australia (bedding@physics.usyd.edu.au)

9 April 2018

ABSTRACT

We report the most sensitive search yet made for solar-like oscillations. We observed the star α Cen A in Balmer-line equivalent widths over six nights with both the 3.9 m Anglo-Australian Telescope and the ESO 3.6 m telescope. We set an upper limit on oscillations of 1.4 times solar and found tentative evidence for p -mode oscillations. We also found a power excess at low frequencies which has the same slope and strength as the power seen from granulation in the Sun. We therefore suggest that we have made the first detection of temporal fluctuations due to granulation in a solar-like star.

Key words: stars: oscillations – Sun: oscillations – Sun: atmosphere – stars: individual: α Cen A (HR 5459) – stars: individual: Procyon (HR 2943)

1 INTRODUCTION

Many attempts have been made to detect stellar analogues of the solar five-minute oscillations. As with helioseismology, it is hoped that the measurement of oscillation frequencies in other stars will place important constraints on stellar model parameters and provide a strong test of evolutionary theory. However, despite several claims in the literature, it is fair to say that there has been no unambiguous detection of solar-like oscillations in any star except the Sun (see reviews by Brown & Gilliland 1994; Kjeldsen & Bedding 1995; Gautschy & Saio 1996; Heasley et al. 1996; Bedding & Kjeldsen 1998).

Most searches for stellar oscillations have used one of two methods: (i) high-resolution spectroscopy, which aims to detect periodic Doppler shifts in spectral features, or (ii) differential CCD photometry, which has been used to search for fluctuations in the integrated luminosity of stars in the open cluster M67 (Gilliland et al. 1993).

We have been using a new method to search for solar-like oscillations that involves measuring temperature changes via their effect on the equivalent widths (EWs) of the Balmer hydrogen lines. We found strong evidence for solar-like oscillations in the G subgiant η Boo (Kjeldsen et al. 1995; Bedding & Kjeldsen 1995), with frequency splittings that were later found to agree with theoretical models (Christensen-Dalsgaard et al. 1995a,b; Guenther & Demarque 1996). Since then, the improved luminosity estimate for η Boo from Hipparcos measurements has given even better agreement (Bedding et al. 1998). However, a search for ve-

locity oscillations in η Boo by Brown et al. (1997) failed to detect a signal, setting limits at a level below the value expected on the basis of the Kjeldsen et al. result. More recently, Brown et al. (in preparation) have obtained a larger set of Doppler observations with lower noise which also fail to show convincing evidence for oscillations.

Meanwhile, the equivalent-width method has now been used to detect oscillations in the spatially resolved Sun (Keller et al. 1998), in the δ Scuti variable FG Vir (Viskum et al. 1998) and in the rapidly oscillating Ap star α Cir (Baldry et al. 1999). For the Sun it has been shown directly that the EW variations of Balmer lines arise because the line intensity oscillates much less than the continuum intensity (Ronan et al. 1991; Keller et al. 1998).

We chose η Boo as the first solar-like target for the EW method because it was expected to have an oscillation amplitude about five times greater than the Sun. This turned out to be the case (assuming the detection is real). We then turned to α Cen A, a more challenging target because of its smaller expected oscillation amplitude (comparable to solar; Bedding et al. 1996). Being a near twin of the Sun and extremely nearby, this star is an obvious target to search for oscillations (e.g., Brown et al. 1994). Previous attempts using Doppler methods were reviewed by Kjeldsen & Bedding (1995). They include two claimed detections at amplitudes 4–6 times greater than solar (Gelly et al. 1986; Pottasch et al. 1992) and two negative results at amplitudes about 2–3 times solar (Brown & Gilliland 1990; Edmonds & Cram 1995).

Here, we report observations of α Cen A in Balmer-line

equivalent widths which set an upper limit of only 1.4 times solar. We find tentative evidence for *p*-mode oscillations. We also find strong evidence for stellar granulation in the power spectrum, at a level consistent with that expected on the basis of solar observations.

2 OBSERVATIONS

We observed α Cen A over six nights in April 1995 from two sites:

- At Siding Spring Observatory in Australia, we used the 3.9-metre Anglo-Australian Telescope (AAT) with the coudé echelle spectrograph (UCLES). We recorded three orders centred at $H\alpha$ and three orders at $H\beta$, which was possible thanks to the flexibility of the CCD controller. The weather was about 85% clear but transparency was variable. The exposure time was typically about 30 s, with a deadtime of 23 s between exposures. This relatively long exposure time for such a bright target was achieved by spreading the light along the spectrograph slit by (i) defocussing the telescope and using a wide slit (5–10 arcsec) and (ii) trailing the star backwards and forwards along the slit with a peak-to-peak amplitude of about 2 arcsec and a period of about 4 s. The slit length was 14 arcsec. Each spectrum typically produced about 9.0×10^7 photons/ \AA in the continuum near $H\alpha$ and about 3.5×10^7 photons/ \AA near $H\beta$.
- At the European Southern Observatory on La Silla in Chile, we used the ESO 3.6-metre telescope with the Cassegrain echelle spectrograph (CASPEC). We recorded three orders centred at $H\alpha$. The weather was 100% clear. The exposure time was typically about 10 s, with a deadtime of 12 s between exposures. The slit was 7 arcsec wide and 10 arcsec long, with slightly less defocus than at the AAT and no trailing. Each spectrum typically produced about 5.5×10^7 photons/ \AA in the continuum near $H\alpha$.

The B component of the α Cen system, which is 1.3 magnitudes fainter than the A component, had a separation of 17.3 arcsec at the time of our observations, so there should not be any contamination. We nevertheless kept the spectrograph slit aligned with the position angle of the binary system so that any light from the B component would be spatially separated on the detector.

In addition to our primary target of α Cen A, we also observed Procyon for one hour at the start of each night, plus 5 hours at both sites at the start of the fifth night. Finally, we observed the solar spectrum via the daytime sky (about 18 hr at AAT and 14 hr at ESO, spread over the six days). For both Procyon and the Sun, this amount of data turned out not to be sufficient to detect oscillations, but we did find evidence for granulation power (see Section 5).

3 DATA PROCESSING

Here we describe the steps involved in processing the data. Section 3.2 is specific to the equivalent-width method, while

the other steps could apply, at least in part, to other types of observations (Doppler shift or photometry).

3.1 Preliminary reduction

- Correction of each CCD frame for bias by subtracting an average bias frame and then subtracting a constant that was measured from the overscan region of the CCD frame.
- Correction for CCD non-linearity. Measuring oscillations at the ppm level requires that the detector be linear to the level of one part in 1000 or better. This cannot be taken for granted and our tests of different CCDs and controllers often reveal deviations from linearity of up to a few per cent. Unless correction is made for these effects, the extra noise will destroy any possibility of detecting oscillations. Both CCDs were Tektronix 1024 \times 1024 chips, used at a conversion factor of about 12 electrons per ADU. The onset of saturation was about 450 000 electrons per pixel for the AAT and 250 000 for ESO. From our measurements, the linearity corrections for both were well approximated by the relation:

$$\text{ADU}_{\text{obs}}/\text{ADU}_{\text{true}} = 1 + \alpha \text{ADU}_{\text{obs}} - \exp(\text{ADU}_{\text{obs}}/\beta + \gamma), \quad (1)$$

where ADU_{obs} and ADU_{true} are observed and true counts measured in ADU and (α, β, γ) had values of $(-1.63 \times 10^{-7}, 700, -59.33)$ for the AAT and $(-2.35 \times 10^{-7}, 700, -33.53)$ for ESO. The measurement error on this correction was one part in 3500.

- Correction for pixel-to-pixel variations in CCD sensitivity by dividing by an average flat-field exposure (all flat-field exposures were corrected for non-linearities before averaging).
- Subtraction of sky background, which was quite substantial during twilight. The background was estimated from the regions at each end of the spectrograph slit, either side of the stellar spectrum in each echelle order.
- Extraction of one-dimensional spectra. During this step, the seeing in each frame (i.e., the FWHM along the spectrograph slit) and the position of the star (i.e., light centroid along the slit) were recorded for use in decorrelation (see Sec. 3.4 below).

3.2 Measuring equivalent widths

Achieving high precision requires more than simply fitting a profile. The method described here was developed after trying several different approaches. By analogy with Strømgren $H\beta$ photometry, we calculated the flux in three artificial filters, one centred on the line (L) and the others on the continuum both redward (R) and blueward (B) of the line. For each spectrum, the following steps were followed:

- Placement of the three filters at their nominal wavelengths.

- (ii) Calculation of the three fluxes B , L and R .*
- (iii) Adjustment of the slope of the spectrum so that R and B were equal. This was done by multiplying the spectrum by a linear ramp.
- (iv) Re-calculation of the filter fluxes and hence of the equivalent width: $W = (R - L)/R$.
- (v) Repetition of steps (ii)–(iv) with the three filters at different positions. Iteration to find the filter position that maximized the value of W . The outputs were: W , the position of the line, the height of the continuum (from R), and slope of continuum.
- (vi) Repetition of steps (i)–(v) for four different filter widths.

The result was four times series (W_1 , W_2 , W_3 , W_4), one for each filter width.

3.3 Initial time series processing

The quality of the data, as measured by the local scatter, varied considerably from hour to hour and night to night. The following procedure was applied to each night of data separately.

- (i) Clipping of each time series to remove outlying points (4σ clipping, where σ is the local rms scatter).
- (ii) Calculation of weights for each time series. This involved assigning a weight to each data point that was inversely proportional to the local variance (σ^2).
- (iii) Calculation of σ_w , the *weighted* rms scatter of each time series, using the weights just calculated. This was used to select the best filter width, i.e., the one which minimized σ_w . By using a weighted rms scatter, we do not give too much importance to the bad segments of the data. In practice, rather than choosing one filter width, we used a weighted combination. That is, we chose the powers a , b , c , d to minimize the weighted scatter on the time series $W_1^a W_2^b W_3^c W_4^d$, where $a + b + c + d = 1$.

This step and the subsequent ones rely on the fact that any oscillation signal will be much smaller than the rms scatter in the time series. Most of the scatter is due to noise and any method of reducing the scatter should be a good thing, although care must be taken not to destroy the signal or to introduce a spurious signal.

3.4 Decorrelation of time series

As well as measuring the parameter which is expected to contain the oscillation signal (W), we also monitored extra parameters. The aim was to correct for instrumental and other non-stellar effects. For example, if W is correlated with the seeing, we would suspect some flaw in the reduction procedure, since the stellar oscillation does not know

what is happening in the Earth's atmosphere. By correlating measured equivalent widths with seeing variations, one has a chance to remove the influence of seeing simply by subtracting that part of the signal which correlates with seeing. This process of decorrelation, which can be repeated for other parameters (total light level, position on detector, slope of continuum, etc.), is very powerful but can also be quite dangerous if not done with care (see Gilliland et al. 1991 for a fuller discussion).

Again, the process was applied to data from one night at a time. Performing decorrelation over shorter intervals runs the risk of moving power around and creating or destroying signal – simulations were useful to check these effects.

Prior to decorrelation, we high-pass filtered the time series to remove low-frequency variations. This was done by subtracting from the time series a smoothed version that was produced by convolution with a supergaussian envelope having a FWHM of 40 minutes.

The AAT spectra included a strong Fe I line near H β at 4383 Å and we used the EW of this line as a decorrelation parameter. This line is temperature sensitive, with the opposite sign and similar amplitude to the Balmer lines (Bedding et al. 1996), so it should contain oscillation signal in anti-phase with the Balmer lines – this was allowed for in the analysis. We found that decorrelating against the Fe I EW gave a significant reduction in the scatter of both the H α and H β EW time series. Unfortunately, the ESO spectra (around H α) did not contain any strong iron lines.

Figure 1 shows the final time series of EW measurements and weights. The data quality clearly varies significantly. Almost one third of the AAT spectra of α Cen A were discarded, although this is not quite as bad as it sounds because many of these were taken well into morning twilight. Still, many night-time AAT spectra were given zero weight. The reason for these poor measurements is not clear, but it is probably related to seeing-induced variations in the point-spread-function through the wide slit (see below). Those AAT measurements that are useful have much lower scatter, and therefore higher weights, than ESO measurements because of the availability of the Fe I line for decorrelation.

4 RESULTS AND SIMULATIONS

The amplitude spectrum of the EW time series was calculated as a weighted least-squares fit of sinusoids (Frandsen et al. 1995; Arentoft et al. 1998), scaled so that a sinusoid with an amplitude of 1 ppm produces a peak of 1 ppm. The power spectrum, the square of this amplitude spectrum, is shown in Figure 2 for the region in which oscillations are expected. No obvious excess of power is seen. We can fit a two-component noise model to the whole power spectrum which consists of (i) white (i.e., flat) noise at a level of 4.3 ppm in the amplitude spectrum, and (ii) a non-white component, which is discussed in Section 5.

The total noise at 2.3 mHz is 4.7 ppm in the amplitude spectrum, while that expected from photon statistics alone

* The flux in a filter is simply the total counts in the stellar spectrum after it has been multiplied by the filter function.

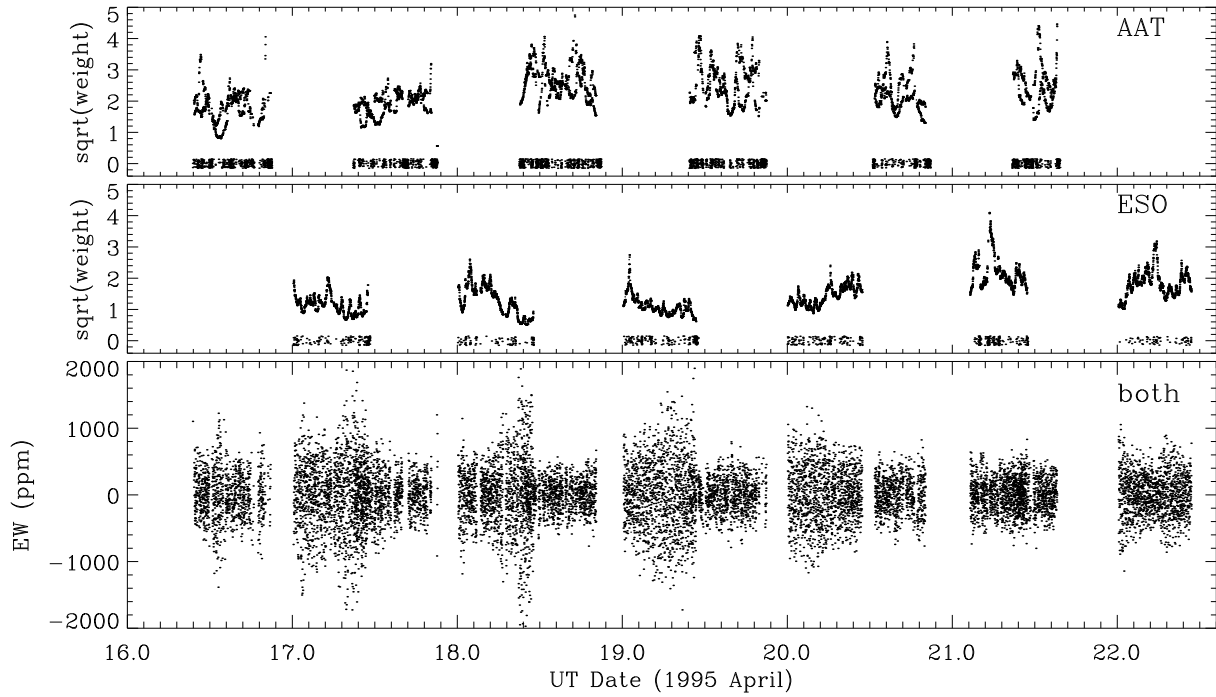


Figure 1. The final time series of EW observations of α Cen A. The upper panel shows the square root of statistical weights (the inverse of the local rms scatter) in arbitrary units for all AAT measurements (both H α and H β are shown). There are 8430 points, with 5773 having non-zero weight. For points with zero weight, we have added a random vertical scatter to make it easier to see their distribution in time. The middle panel shows the same for ESO data (H α only); there are 8847 points, with 7999 having non-zero weight. The bottom panel shows all EW measurements having non-zero weight (13772 points). The peak-to-peak height of the individual modes we are trying to detect corresponds approximately to the size of the dots in the figure.

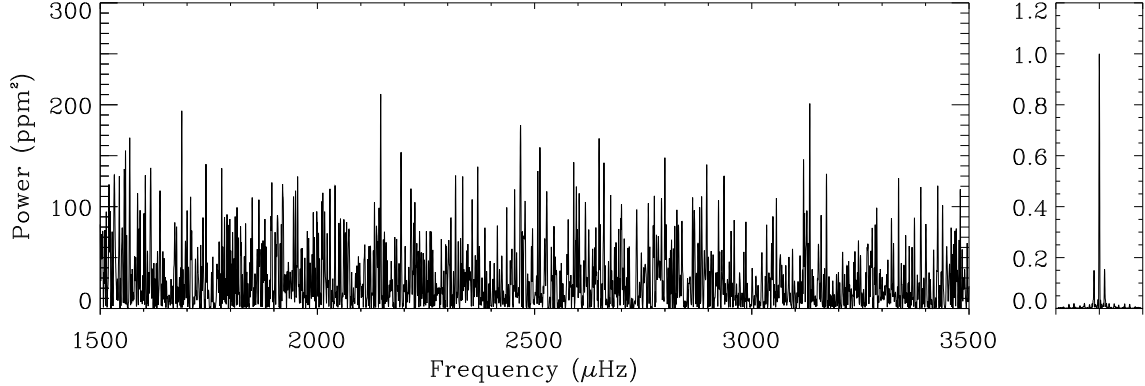


Figure 2. Power spectrum of equivalent-width observations of α Cen A in the region where signal would be expected. The right-hand plot shows the spectral window, with the same horizontal scale, calculated by taking the power spectrum of a sinusoid with an amplitude of 1 ppm and the same sampling and weights as the actual data.

is 2.4 ppm. We are therefore a factor of 1.8 away from the photon noise, with the extra noise presumably coming from instrumental and/or atmospheric effects. The use of a wide slit, while advantageous in terms of exposure times and duty cycle, led to seeing-induced changes in the point-spread-function which may be the cause.

4.1 Simulations

We expect oscillations in α Cen A to produce a regular series of peaks in the power spectrum, with amplitudes modulated by a broad envelope centred at about 2.3 mHz (Kjeldsen &

Bedding 1995). The average amplitude of oscillation modes near the peak of this envelope, as measured in Balmer line EW, is expected to be about 8 ppm, which is 1.4 times that for the Sun (Bedding et al. 1996). To investigate whether an oscillation signal may be present in our data, we have generated simulated time series consisting of artificial signal plus noise. Each simulated series had exactly the same sampling function and allocation of statistical weights as the real data. The injected signal contained sinusoids at the frequencies calculated by Edmonds et al. (1992) for modes with $\ell = 0$ to 3, modulated by a broad solar-like envelope centred at 2.3 mHz and with a central height of 8 ppm. In each

simulation, the phases of the oscillation modes were chosen at random and the amplitudes were randomized about their average values. All these characteristics were chosen to imitate as closely as possible the stochastic nature of oscillations in the Sun. Before calculating each power spectrum, we added normally-distributed noise to the time series, so as to produce a noise level in the amplitude spectrum of 4.7 ppm (consistent with the actual data).

Some results are shown in Figure 3. The top panel shows a simulation without any added noise; the randomization of mode amplitudes within the broad envelope is clear. The next five panels show simulations with noise included (each with different randomization of noise, mode amplitudes and mode phases), while the bottom panel shows the actual data.

It is interesting to note that some of the signal peaks in the simulations have been strengthened significantly by constructive interference with noise peaks. For example, a signal peak of 8 ppm which happens to be in phase with a 2σ noise peak (2×4.7 ppm) will produce a peak in power of 300 ppm². This illustrates the point made by Kjeldsen & Bedding (1995; Appendix A.2): the effects of noise must be taken into account when estimating the amplitude of a signal.

In these five simulations we can see that a signal of 8 ppm is sometimes obvious but sometimes not. To quantify this, we have looked at the eight strongest peaks in each power spectrum in the frequency range 1600–3000 μ Hz. These are marked by vertical lines in Figure 3. Dotted lines show peaks that coincide with input frequencies or their 1/day aliases to within $\pm 1.3 \mu$ Hz (which is twice the rms scatter on the differences between input and measured frequencies). The remaining peaks, marked by dashed lines, are assumed to be due to noise. The results show that 2–5 of the eight strongest peaks coincided with input frequencies and a further 0–2 were 1/day aliases (the mean values for these were 4.0 and 1.0, respectively).

The same information is shown in Figure 4 in the form of echelle diagrams. The top panel shows all input frequencies from Edmonds et al. (1992), although most of these are given very small amplitudes in the simulations. The symbols indicate different ℓ values: 0 (squares), 1 (triangles), 2 (diamonds) and 3 (crosses). The next five panels show the eight strongest peaks in each simulation. The solid lines show the loci of input model frequencies. Each peak in Figure 3 is identified either as noise (asterisks) or as one of the input frequencies. In the latter case, some peaks are shifted by 1/day (11.57μ Hz), as indicated by dotted lines.

4.2 Mode identifications

Given that some of the eight strongest peaks in our power spectrum of α Cen A may be real, we can attempt to identify the modes to which they correspond. Mode frequencies for low-degree and high-order oscillations in the Sun and other solar-like stars are well approximated by the asymptotic relation:

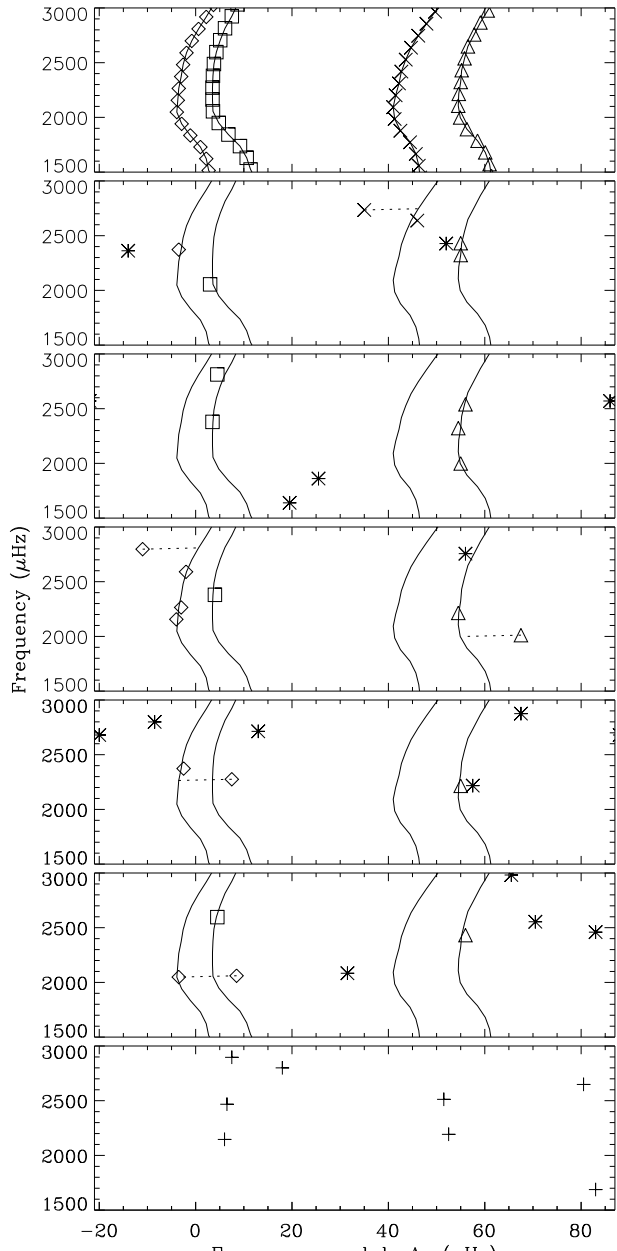


Figure 4. Echelle diagrams based on Figure 3. The top panel shows the input model frequencies, plotted using $\Delta\nu = 108.0 \mu\text{Hz}$. The symbols indicate different ℓ values: 0 (squares), 1 (triangles), 2 (diamonds) and 3 (crosses). The next five panels show the eight strongest peaks in each simulation. The solid lines show the locus of input model frequencies. Each peak is identified either as noise (asterisks) or as one of the input frequencies. In the latter case, some peaks are shifted by 1/day ($11.57 \mu\text{Hz}$), as indicated by dotted lines. The bottom panel shows the eight strongest peaks in the actual data, with $\Delta\nu = 107.0 \mu\text{Hz}$.

$$\nu(n, \ell) = \Delta\nu(n + \frac{1}{2}\ell + \varepsilon) - \ell(\ell + 1)D_0. \quad (2)$$

Here n and ℓ are integers which define the radial order and angular degree of the mode, respectively; $\Delta\nu$ (the so-called large separation) reflects the average stellar density, D_0 is sensitive to the sound speed near the core and ε is sensitive to the surface layers. Values for these three parameters in the

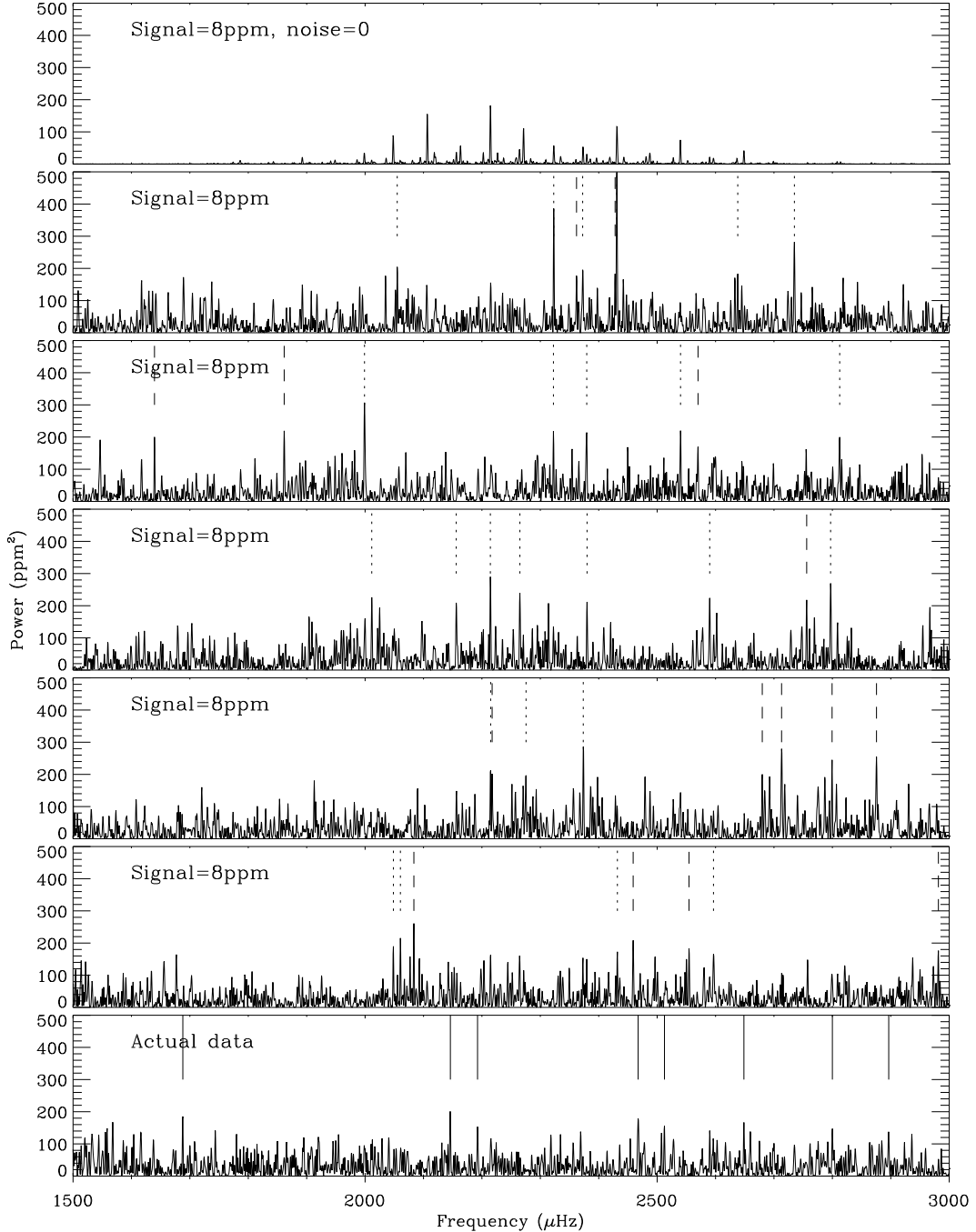


Figure 3. Simulated power spectra for α Cen A, using the same sampling times and data weights as the actual observations. The top panel shows a simulation without noise, while the next five panels show simulations with noise. The eight strongest peaks are marked by vertical lines, with dotted lines indicating those coinciding with input frequencies or their 1/day aliases, and dashed lines showing noise peaks (see also Figure 4). The bottom panel shows the actual data from α Cen A, with the eight strongest peaks being marked (see Table 1).

Sun are:

$$\begin{aligned}\Delta\nu &= 135.12 \pm 0.18 \mu\text{Hz} \\ D_0 &= 1.50 \pm 0.03 \mu\text{Hz} \\ \varepsilon &= 1.46 \pm 0.03\end{aligned}$$

We obtained these values by fitting Equation 2 to solar frequency measurements for $n = 17\text{--}25$ and $\ell = 0\text{--}2$ by Fröhlich et al. (1997).

The curvature in the Edmonds et al. (1992) frequencies for α Cen A, obvious in Figure 4, indicates a departure from the asymptotic theory. Curvature is also predicted by models of the Sun, at a level larger than actually observed, reflecting the difficulty in modelling the solar surface. Therefore, the real oscillation frequencies in α Cen A are also likely to show less curvature than the model by Edmonds et al. This does not affect the conclusions of the simulations, but

Table 1. Frequencies of the eight strongest peaks in the α Cen power spectrum and possible mode identifications (n, ℓ).

Frequency (μ Hz)	Case 1	Case 2	Possible identifications	Case 4
			Case 3	
1687.79	$\nu(13, 3) - 1/d?$	noise	$\nu(15, 1)$	$\nu(14, 2)$
2145.76	$\nu(18, 1)$	$\nu(18, 2)$	$\nu(20, 0)$	$\nu(19, 1)$
2192.55	$\nu(18, 2)$	$\nu(18, 3)$	$\nu(20, 1)$	$\nu(19, 2)$
2467.68	$\nu(21, 1)$	$\nu(21, 2)$	noise	noise
2512.35	$\nu(21, 2)$	$\nu(21, 3)$	noise	$\nu(23, 0) + 1/d?$
2648.48	$\nu(22, 3) - 1/d?$	noise	$\nu(25, 0)$	$\nu(24, 1)$
2799.92	$\nu(24, 1) + 1/d?$	$\nu(24, 2) + 1/d?$	noise	noise
2896.28	$\nu(25, 1)$	$\nu(25, 2)$	$\nu(27, 1)$	$\nu(26, 2)$
$\Delta\nu/\mu$ Hz	106.94 ± 0.13	106.99 ± 0.16	100.77 ± 0.17	100.77 ± 0.17
D_0/μ Hz	2.05 ± 0.05	1.35 ± 0.09	1.95 ± 0.29	1.07 ± 0.09
ε	1.61 ± 0.03	1.14 ± 0.04	1.29 ± 0.04	1.81 ± 0.04

is important when we try to assign modes to our observed frequencies.

The bottom panel of Figure 3 shows the eight strongest peaks in the actual data. Assuming our representation of the mode amplitudes in α Cen A is realistic, we would expect some of these to correspond to actual frequencies. We have therefore searched for values of $\Delta\nu$ which fit the observed frequencies, as follows. We calculated all pairwise differences and looked for a value of $\Delta\nu$ which agreed with as many of these as possible (within $\pm 0.8 \mu$ Hz). The only two values of $\Delta\nu$ in the range 96 – 116μ Hz which gave four or more coincidences were 100.8μ Hz (6 pairs) and 107.0μ Hz (5 pairs). We also checked how well randomly chosen frequencies gave similar coincidences. On the basis of 25 simulations, we found that 6 coincidences occurred only once.

For both of the values of $\Delta\nu$ found above, we attempted to identify each of the eight observed frequencies by fitting to Equation 2. There are two possible identifications for each value of $\Delta\nu$ that have D_0 in a physically realistic range (0.7 – 3.0μ Hz; Christensen-Dalsgaard 1993) and these are given in Table 1. We chose n such that ε lay in the range 1–2.

We stress that we do not claim to have detected oscillations but that, if we have, one of the four cases in the table represents the most likely description. In that case, the implied amplitude is 7–8 ppm (1.3 times solar). If none of the eight frequencies is real, the oscillations must be below 7 ppm (1.2 times solar). Either way, these observations represent the most sensitive search yet made for stellar variability.

5 GRANULATION POWER

The power spectrum of full-disk intensity measurements of the Sun shows a sloping background due to granulation and other surface structure (e.g., Rabello Soares et al. 1997). This power background reflects surface temperature fluctuations, so we expect it also to be present in EW measurements. Indeed, our power spectrum of α Cen A (Figure 5) shows an excess at low frequencies. The same is true for our observa-

tions of Procyon and the Sun, although there are much less data.

Note that the power density scales on the right-hand axes were obtained by multiplying the left-hand scales (defined in Section 4) by the effective timespan of the observations (see Appendix A.1 of Kjeldsen & Bedding 1995). For α Cen A, for example, the observations spanned 145 hr from start to finish. However, the measurements were given different weights, so we calculated the effective timespan by integrating under the weighted spectral window (right panel in Figure 2); the result was 85.5 hr. It is important to note that published power density spectra are often calculated using different versions of Parseval's theorem and must be multiplied by either two or four to be compared with our definition of power density.

To investigate whether the low-frequency power excess observed in α Cen A could arise from stellar granulation, we must make two corrections. Firstly, we must subtract the contribution from white noise (photon noise, instrumental and atmospheric effects), which we measure to have a level of $7.3 \pm 0.2 \text{ ppm}^2/\mu\text{Hz}$. This is shown by the horizontal line in Figure 5. Secondly, at frequencies below about $800 \mu\text{Hz}$ there is a deficit of power due to the high-pass filter (see Section 3.4).

The thick solid line in Figure 6 shows the power density from our EW measurements of α Cen A after subtraction of the constant white noise term, correction for high-pass filtering and smoothing. The two thinner solid lines on either side show the $\pm 2\sigma$ errors in the two corrections.

The power is quite uncertain at low frequencies due to uncertainties in the removal of the effects of the high-pass filter, and at high frequencies due to uncertainties in the subtraction of white noise component. At intermediate frequencies (600 – 3000μ Hz), our measurement should be accurate and in this regime the power is linear and well described by the following relation:

$$\log(\text{power density}) = G + P \log\left(\frac{\nu}{1 \text{ mHz}}\right) \quad (3)$$

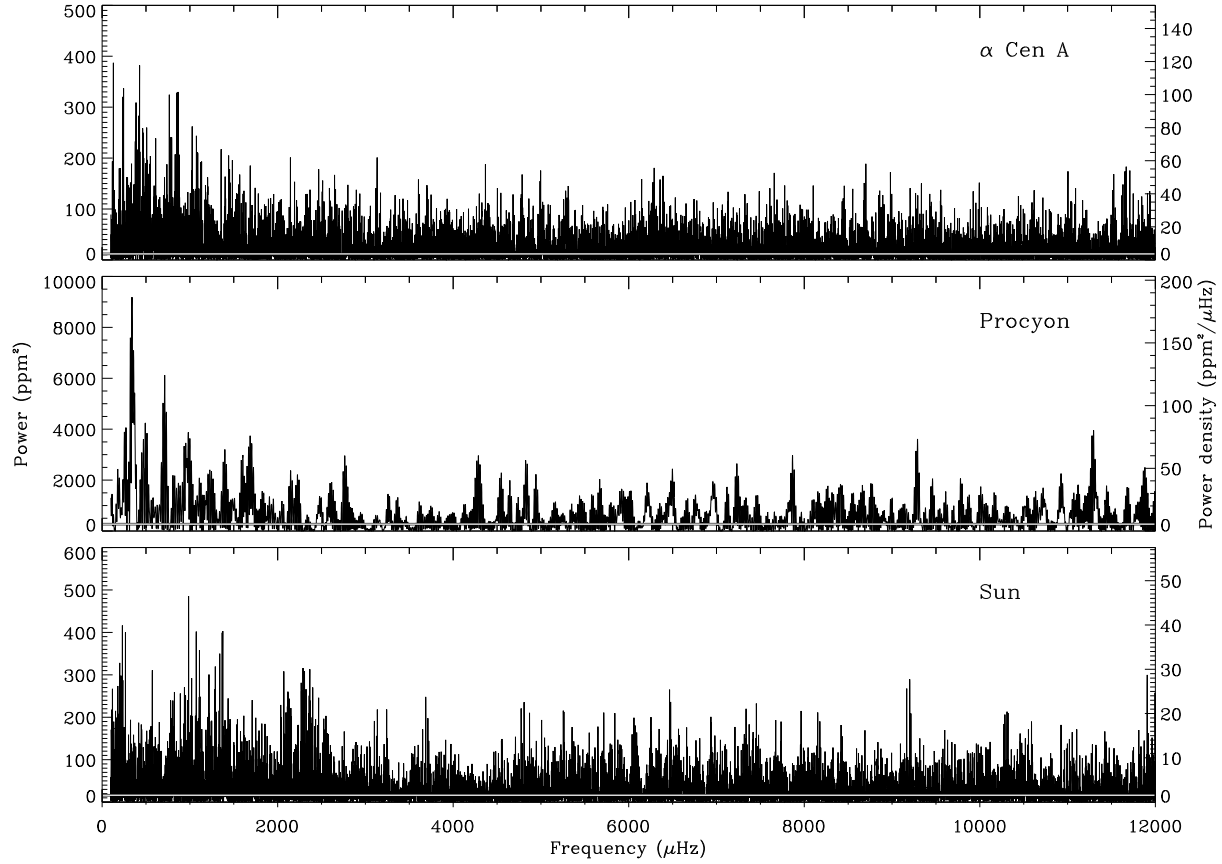


Figure 5. Power spectra of equivalent-width observations of α Cen A, Procyon and the Sun. In each case, the mean level of white noise is shown by the horizontal white line.

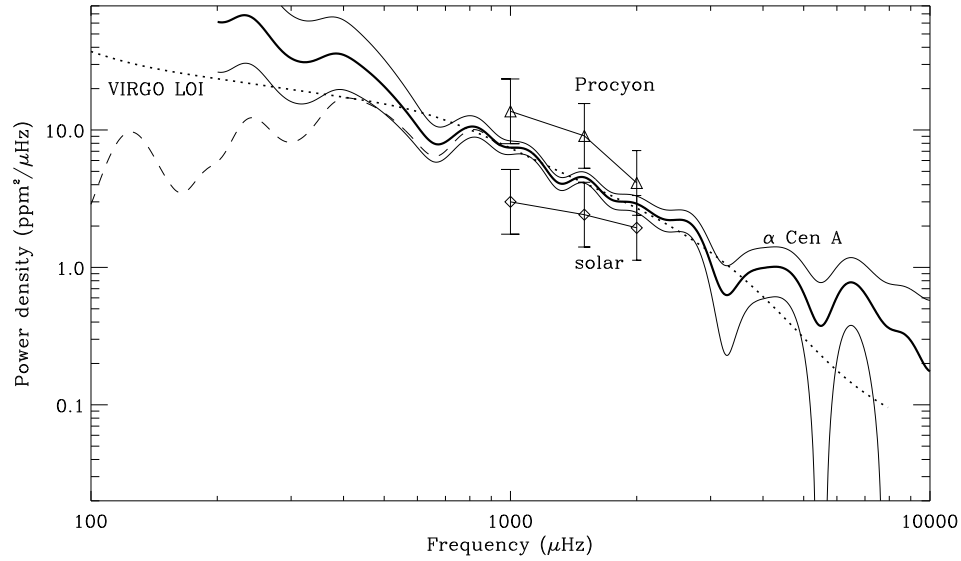


Figure 6. Comparison of power density spectra. The thick solid curve shows the observed EW power density from our AAT/ESO observations of α Cen A, after subtraction of white noise and after correction at low frequencies for the effect of the high-pass filter. The two thinner solid lines on either side show the $\pm 2\sigma$ errors in these two corrections. Dashed curve: same as thick solid curve, but without correction for the high-pass filter. The symbols show EW measurements from our AAT/ESO observations for Procyon and the Sun, with 2σ error bars. The dotted line shows our estimate of the EW granulation power density in the Sun, scaled from published intensity measurements by the VIRGO LOI instrument (see text).

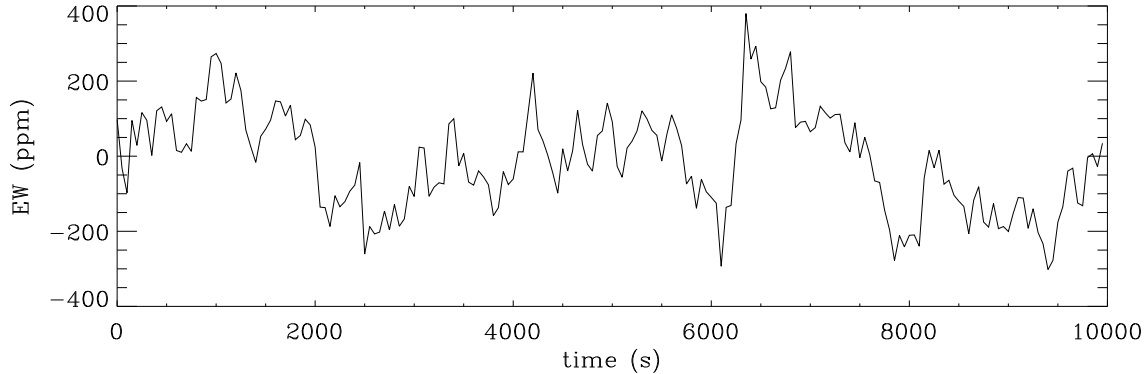


Figure 7. Example time series for EW measurements of α Cen A based on the non-white component of the power spectrum.

where

$$G = 0.85 \pm 0.09$$

$$P = -1.46 \pm 0.15$$

and the power density is measured in $\text{ppm}^2/\mu\text{Hz}$. The slope of the background power is very similar to that produced by solar granulation (e.g., Rabello Soares et al. 1997). To compare the amount of power in our EW measurements with published measurements of the total solar intensity, we must estimate the conversion factor between the two observing methods. For the Sun, a fractional change in intensity of 1 ppm that is caused by a temperature change corresponds to a change in EW of the Balmer lines of 1.5 ppm (Bedding et al. 1996). We assume the same conversion factor applies to temperature fluctuations from granulation. Furthermore, the amount of limb darkening in the EW of Balmer lines – and hence the signal from granulation – is greater than in total intensity (Bedding et al. 1996) by a factor which we estimate to be 1.15. Hence, published measurements of the power density of solar intensity should be multiplied by $(1.5)^2(1.15)^2 = 3.0$.

We have applied this conversion to the recent measurement of full-disk solar intensity measurements made with the LOI (Luminosity Oscillations Imager) part of the VIRGO instrument on the SOHO spacecraft (Fig. 2 of Appourchaux et al. 1997). The result is shown as the dotted line in Figure 6. Note that it was also necessary to multiply the LOI values by four to bring them into line with our definition of power density (T. Appourchaux, private communication). The agreement with our observations of α Cen A is excellent, giving strong evidence that we have detected stellar granulation.

Our observations of Procyon and the daytime sky also produced power spectra with excesses at low frequencies (Figure 5). These power levels are shown in Figure 6, with 2σ error bars. Our solar measurement is in reasonable agreement with the LOI data, although slightly too low. The granulation power in Procyon appears to be greater than that in α Cen A by a factor of 2.0, although this result is only at the 2σ level.

To illustrate the size of the granulation signal from α Cen A, we show in Figure 7 an example time series, sam-

pled at 50 s intervals, based on the non-white component of the power spectrum (the thick line in Figure 6). This is how the EW signal from α Cen would look without photon noise or measurement errors.

When one is trying to detect oscillations, these fluctuations in EW due to stellar granulation represent a fundamental noise source. For example, suppose that the weather had been 100% clear and that all of our EW measurements ($\text{H}\alpha$ and $\text{H}\beta$) were photon-noise limited. Then we would have expected a white noise level in the amplitude spectrum (from photon noise) of 1.4 ppm and a noise level from granulation at 2.3 mHz of 1.9 ppm. The total noise at 2.3 mHz would then have been 2.4 ppm, about half the value that we actually measured. In other words, we were a factor of two away from the limit set by photon and granulation noise, presumably due to instrumental and atmospheric effects. Had we achieved this limit, a signal with solar amplitude (about 6 ppm) would have been detected.

Given a CCD with sufficiently fast readout, it would be possible to record a much larger part of the spectrum and hence to measure EWs of many more lines at a higher duty cycle (Bedding et al. 1996). The photon noise would then be reduced by up to a factor of about two, to which granulation noise must still be added. This represents the fundamental limit for the EW method.

Granulation is also a fundamental limit for intensity and colour measurements, but much less critically for Doppler shift measurements, since the background power in the solar velocity spectrum is a tiny fraction of the oscillation amplitudes (Gabriel et al. 1997).

6 CONCLUSIONS

Our observations of α Cen A represent the most sensitive search yet made for solar-like oscillations. We can set a firm upper limit on the amplitudes of 1.4 times solar, which is approximately the level at which oscillations are expected. We find tentative evidence for p modes in the form of a regular series of peaks. If these do not correspond to real oscillations then the upper limit on amplitude becomes 1.2 times solar.

We find an excess of power at low frequencies in

α Cen A which has the same slope and strength as power from granulation in the Sun. We therefore suggest that we have made the first detection of granulation power in a solar-like star.

ACKNOWLEDGEMENTS

The observations would have been impossible without the excellent support we received from staff at both observatories. We are especially grateful to Roy Antaw, Bob Dean, Sean Ryan, John Stevenson and Gordon Shafer at the AAO and to Luca Pasquini, Peter Sinclair and Nicolas Haddad at ESO. We also thank both committees (ATAC and OPC) for allocating telescope time and the AAO Director for granting the sixth AAT night. This work was supported financially by the Australian Research Council, by the Danish Natural Science Research Council and by the Danish National Research Foundation through its establishment of the Theoretical Astrophysics Center.

References

Appourchaux, T., Andersen, B. N., Fröhlich, C., Jiménez, A., Telljohann, U., & Wehrli, C., 1997, *Sol. Phys.*, 170, 27

Arentoft, T., Kjeldsen, H., Nuspl, J., Bedding, T. R., Fronto, A., Viskum, M., Frandsen, S., & Belmonte, J. A., 1998, *A&A*, 338, 909

Baldry, I. K., Viskum, M., Bedding, T. R., Kjeldsen, H., & Frandsen, S., 1999, *MNRAS* (in press)

Bedding, T. R., & Kjeldsen, H., 1995. In: Stobie, R. S., & Whitelock, P. A. (eds.), *IAU Colloquium 155: Astrophysical Applications of Stellar Pulsation*, Vol. 83 of *A.S.P. Conf. Ser.*, p. 109, Utah: Brigham Young

Bedding, T. R., & Kjeldsen, H., 1998. In: Donahue, R. A., & Bookbinder, J. A. (eds.), *Proc. Tenth Cambridge Workshop on Cool Stars, Stellar Systems and the Sun*, Vol. 154 of *A.S.P. Conf. Ser.*, p. 301, San Francisco: ASP

Bedding, T. R., Kjeldsen, H., Reetz, J., & Barbuy, B., 1996, *MNRAS*, 280, 1155

Bedding, T. R., Kjeldsen, H., & Christensen-Dalsgaard, J., 1998. In: Donahue, R. A., & Bookbinder, J. A. (eds.), *Poster Proc. Tenth Cambridge Workshop on Cool Stars, Stellar Systems and the Sun*, pp. CD-741, San Francisco: ASP (astro-ph/9709005)

Brown, T. M., & Gilliland, R. L., 1990, *ApJ*, 350, 839

Brown, T. M., & Gilliland, R. L., 1994, *ARA&A*, 33, 37

Brown, T. M., Christensen-Dalsgaard, J., Weibel-Mihalas, B., & Gilliland, R. L., 1994, *ApJ*, 427, 1013

Brown, T. M., Kennelly, E. J., Korzennik, S. G., Nisenson, P., Noyes, R. W., & Horner, S. D., 1997, *ApJ*, 475, 322

Christensen-Dalsgaard, J., 1993. In: Brown, T. M. (ed.), *GONG 1992: Seismic Investigation of the Sun and Stars*, Vol. 42 of *A.S.P. Conf. Ser.*, p. 347, Utah: Brigham Young

Christensen-Dalsgaard, J., Bedding, T. R., Houdek, G., Kjeldsen, H., Rosenthal, C., Trampedach, R., Monteiro, M., & Nordlund, Å., 1995a. In: Stobie, R. S., & Whitelock, P. A. (eds.), *IAU Colloquium 155: Astrophysical Applications of Stellar Pulsation*, Vol. 83 of *A.S.P. Conf. Ser.*, p. 447, Utah: Brigham Young

Christensen-Dalsgaard, J., Bedding, T. R., & Kjeldsen, H., 1995b, *ApJ*, 443, L29

Edmonds, P. D., & Cram, L. E., 1995, *MNRAS*, 276, 1295

Edmonds, P. D., Cram, L. E., Demarque, P., Guenther, D. B., & Pinsonneault, M., 1992, *ApJ*, 394, 313

Frandsen, S., Jones, A., Kjeldsen, H., Viskum, M., Hjorth, J., Andersen, N. H., & Thomsen, B., 1995, *A&A*, 301, 123

Fröhlich, C., Andersen, B. N., & Appourchaux, T., et al., 1997, *Sol. Phys.*, 170, 1

Gabriel, A. H., Charra, J., & Grec, G., et al., 1997, *Sol. Phys.*, 175, 207

Gautschy, A., & Saio, H., 1996, *ARA&A*, 34, 551

Gelly, G., Grec, G., & Fossat, E., 1986, *A&A*, 164, 383

Gilliland, R. L., Brown, T. M., Ducan, D. K., Suntzeff, N. B., Lockwood, G. W., Thompson, D. T., Schild, R. E., Jeffrey, W. A., & Penprase, B. E., 1991, *AJ*, 101, 541

Gilliland, R. L., Brown, T. M., Kjeldsen, H., McCarthy, J. K., Peri, M. L., Belmonte, J. A., Vidal, I., Cram, L. E., Palmer, J., Frandsen, S., Parthasarathy, M., Petro, L., Schneider, H., Stetson, P. B., & Weiss, W. W., 1993, *AJ*, 106, 2441

Guenther, D. B., & Demarque, P., 1996, *ApJ*, 456, 798

Heasley, J. N., Janes, K., Labonte, B., Guenther, D., Mickey, D., & Demarque, P., 1996, *PASP*, 108, 385

Keller, C. U., Harvey, J. W., Barden, S. C., Giampapa, M. S., Hill, F., & Pilachowski, C. A., 1998. In: Deubner, F.-L., Christensen-Dalsgaard, J., & Kurtz, D. W. (eds.), *Proc. IAU Symp. 185, New Eyes to See Inside the Sun and Stars*, p. 375, Dordrecht: Kluwer

Kjeldsen, H., & Bedding, T. R., 1995, *A&A*, 293, 87

Kjeldsen, H., Bedding, T. R., Viskum, M., & Frandsen, S., 1995, *AJ*, 109, 1313

Pottasch, E. M., Butcher, H. R., & van Hoesel, F. H. J., 1992, *A&A*, 264, 138

Rabello Soares, M. C., Roca Cortés, T., Jiménez, A., Andersen, B. N., & Appourchaux, T., 1997, *A&A*, 318, 970

Ronan, R. S., Harvey, J. W., & Duvall, Jr., T. L., 1991, *ApJ*, 369, 549

Viscum, M., Kjeldsen, H., Bedding, T. R., Dall, T. H., Baldry, I. K., Bruntt, H., & Frandsen, S., 1998, *A&A*, 335, 549

This paper has been produced using the Blackwell Scientific Publications *LATEX* style file.